Batch Fabrication of Customizable Silicone-Textile Composite Capacitive Strain Sensors for Human Motion Tracking

*Asli Atalay, Vanessa Sanchez, Ozgur Atalay, Daniel M. Vogt, Florian Haufe, Robert J. Wood, and Conor J. Walsh**

This paper presents design and batch manufacturing of a highly stretchable textile-silicone capacitive sensor to be used in human articulation detection, soft robotics, and exoskeletons. The proposed sensor is made of conductive knit fabric as electrode and silicone elastomer as dielectric. The batch manufacturing technology enables production of large sensor mat and arbitrary shaping of sensors, which is precisely achieved via laser cutting of the sensor mat. Individual capacitive sensors exhibit high linearity, low hysteresis, and a gauge factor of 1.23. Compliant, low-profile, and robust electrical connections are established by fusing filaments of micro coaxial cable to conductive fabric electrodes of the sensor with thermoplastic film. The capacitive sensors are integrated on a reconstructed glove for monitoring finger motions.

There is an increased demand for soft sensors for continuous monitoring of body movements,[1–8] for use in human–machine interfaces,[9–12] and for measuring physiological parameters of the human body.[13–17] Soft sensors provide the ability to obtain accurate measurements close to the human body in a comfortable manner and are straightforward to integrate into wearable garments. To date, resistive[18–21] and capacitive[7,22–25] soft sensors have dominated research in this field due to ease of readout electronics and general compatibility with soft materials.

Strain sensors are evaluated by several performance parameters, that is, stretchability, sensitivity or gauge factor (GF), linearity, hysteresis, response time, drift and dynamic durability, and overshooting behavior. High stretchability was observed for both resistive sensors and capacitive sensors through approaches such as utilizing stable electromechanical characteristics of 1D nanomaterials,[26,27] using fibrous structured conductive materials[28] or creating microstructured surface treatments (such as buckling for strain relief).[29] The GF of resistive strain sensors can go beyond 1000 due to mechanisms such as dense microcrack generation at the expense of reduced stretchability (30% and below)[30] or lower gauge factor with increased maximum strain level.[31] Capacitive sensors exhibit low sensitivity and it is described in previous work that their maximum GF value is 1. For instance, it is experimentally shown that silver nanowires (AgNWs)-Ecoflex and CNT capacitive sensors exhibit 1 and 0.5 GF, respectively.[25,32] The linearity performance of a sensor is important for the calibration process. Despite their high gauge factor, most resistive sensors exhibit nonlinear behavior[8] due to a nonhomogeneous change within the sensing structure under applied strain,[33,34] while capacitive sensors exhibit excellent linearity.[27,35] Additionally, capacitive sensors have improved hysteresis and response times compared to resistive sensors, which is valuable for wearable applications where sensors undergo repeated dynamic strains.[27,36] Both parameters are related to the effect of the viscoelastic nature of polymers in the working mechanism of the sensors; a resistive sensor[33] and a capacitive sensor[35] comprised of AgNWs have response times of 200 and 40 ms, respectively. Both types of sensors exhibit overshooting behavior,[26,27] however, resistive strain sensors exhibit larger overshooting when compared to capacitive strain sensors.[8] Dynamic durability and drifting behavior over time were investigated and good performance was reported for both capacitive and resistive-based sensors.[26,27] Despite the advantages of capacitive sensors, they are prone to EM interference and fringe fields from anything conductive (including biological entities).[35] This interference can be eliminated by shielding the sensor, with a tradeoff of increased sensor thickness due to additional layers.

Capacitive-based soft sensors can be constructed using two conformable electrodes with a dielectric layer in between. A capacitance change occurs when the two main parameters, electrode area and dielectric thickness, change geometry in response to applied strain. Existing attempts for developing stretchable and soft capacitive sensors can be classified as textile-based or silicone-based approaches. Silicone-based sensors can be developed by employing conductive elements made from nanomaterials, that is, nanowires,[22,37,38] liquid metals,[7,21] carbon nanotubes,[4,39–41] graphene,[42–46] and carbon

Dr. A. Atalay, V. Sanchez, Dr. O. Atalay, D. M. Vogt, F. Haufe, Prof. R. J. Wood, Prof. C. J. Walsh
John A. Paulson School of Engineering and Applied Sciences
Harvard University
29 Oxford Street, Cambridge, MA 02138, USA
E-mail: walsh@seas.harvard.edu
Dr. A. Atalay, V. Sanchez, Dr. O. Atalay, D. M. Vogt, F. Haufe, Prof. R. J. Wood, Prof. C. J. Walsh
Wyss Institute for Biologically Inspired Engineering at Harvard
3 Blackfan Circle, Boston, MA 02115, USA

DOI: 10.1002/admt.201700136

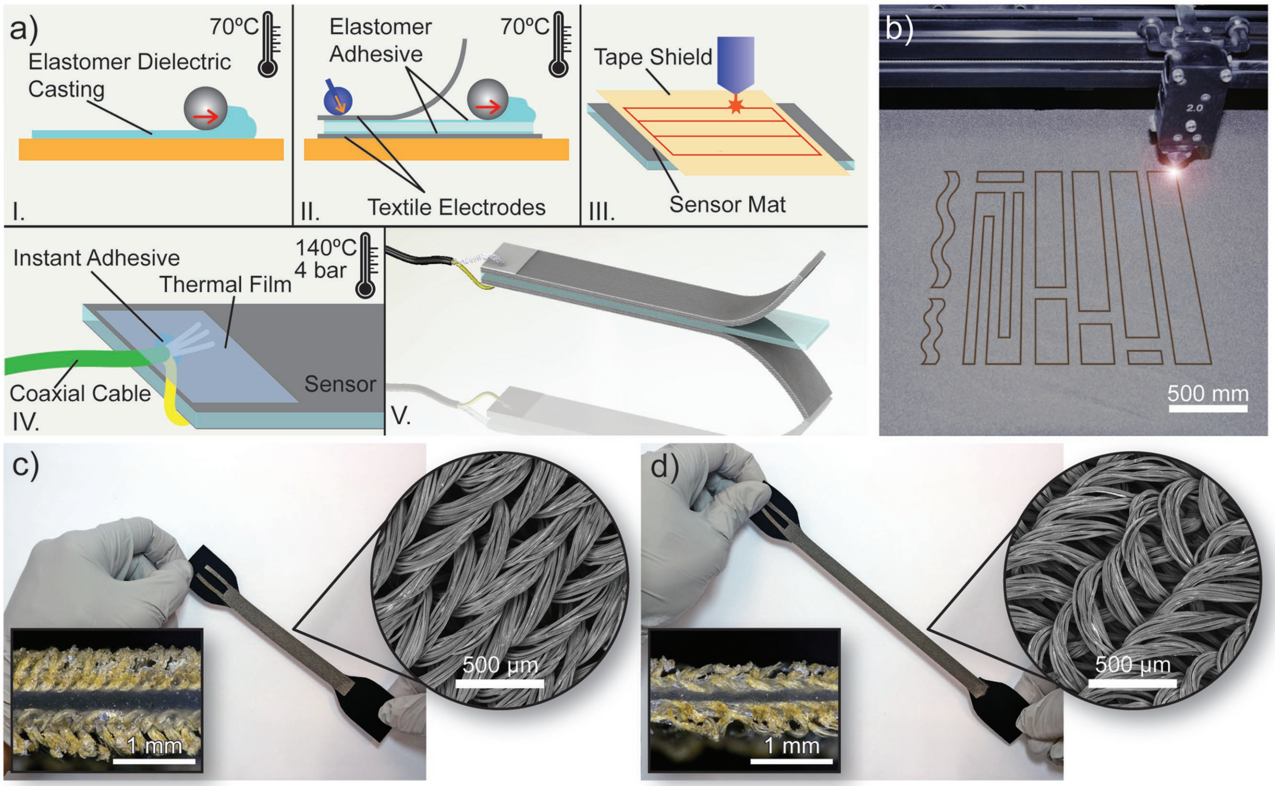

Figure 1. a) Schematic diagram of the fabrication process of the composite textile-silicone sensor: (i) Dielectric silicone casting. (ii) Bonding of fabric electrodes via silicone elastomer casting. (iii) Placement of tape shield and laser cutting of sensor. (iv) Creation of permanent electrical connection between coaxial cable and fabric electrode using instant adhesive and thermal film. (v) 3D illustration of the sensor and material layers. b) Schematic diagram of arbitrary shaping of sensors via laser cutting. c,d) Photos of the sensor illustrating application of stretching at ≈0 and 100% strain; insets: cross-section views; popouts: surface views.

black[19,47,48] for the construction of the electrode and silicone elastomer as the dielectric. Textile-based capacitive sensors can be manufactured by embedding conductive yarns into the textile structure via knitting, weaving, or embroidery techniques or top-applied via printing or coating.[23,49–53] However, both technologies, that is, textile-based and silicone-based, have their own individual limitations. Textile-based sensors suffer from poor elastic operation range, low baseline capacitance values, and are susceptible to mechanical friction with high hysteresis.[50] They are primarily used for pressure-sensing applications.[23,24,48–55] Silicone-based sensors have low sensitivity (gauge factor), and complex manufacturing processes, including the preparation of masks, patterning, and chemical reactions to create electrodes.[56–58] Their delicate conductive network of electrodes and low adhesion between the electrode and dielectric can lead to delamination.[29,45,59] Furthermore, difficulties connecting to readout electronics create system integration challenges.[4,7] One of the main challenges is to create soft and robust connections on soft sensors. There are some studies that investigate employing liquid metals to construct soft and stretchable connections; however, this can create challenges for integration.

To address these limitations, we propose a hybrid approach (i.e., combining textiles and silicone) for capacitance-based soft sensing. Specifically, we present a scalable batch manufacturing process by constructing electrodes from a conductive knit fabric and the dielectric layer from a silicone elastomer as shown in **Figure 1**. The favorable mechanical properties of the composite textile and silicone elastomer structure address the issues of poor elastic operation range and low GF. We also introduce a flexible and robust electrical connection method using thermal bonding. We demonstrate that the sensor exhibits linear output and increased elastic operation range compared with textile-based capacitive sensors, more robustness when compared to silicone-based capacitive sensors, as well as a high baseline capacitance and increased sensitivity relative to both technologies. A high baseline capacitance gives the sensors robustness to parasitic capacitance in the readout circuitry, and therefore an improved signal-to-noise ratio.[55]

Our layered batch manufacturing process, as described in detail below using an automatic film applicator, allows for rapid, robust, reliable, and scalable production of large sensor sheets. The laser cutting process enables the creation of arbitrary, customizable individual sensors. Specifically, the sensor is made of two electrode layers of highly stretchable silver-plated knitted textile (Shieldex Medtex-130, V Technical Textiles Inc., USA) and separated by a silicone elastomer (Ecoflex 00-30, SmoothOn Inc., USA) as the dielectric.

We fabricate our sensors in a bulk layer-based production methodology via combining the conductive knitted fabric with silicone as illustrated in Figure 1a (see also Movie S1, Supporting Information). First, a film of silicone is cast and cured as the dielectric layer. The conductive textile is then adhered to each surface through the application of a thinner casting of silicone, application of the textile on the surface with pressure applied via a roller. This produces an entire bulk sheet of sensor that can then have sensors of arbitrary shape cut from it precisely with a laser (Figure 1a,b and Movie S2, Supporting Information). An additional advantage of this approach is that identical sensors cut from the same sheet can have consistent baseline capacitance values. For example, five samples from one such mat (with the dimensions of 80 mm × 100 mm × 0.102 mm) had 174 pF ± 1.41 as values for their initial capacitance. The laser cutting process also singes fibers at the conductive fabric edges preventing shorting of the electrodes (as opposed to cutting with a blade where the top and bottom electrode can easily short due to crossing of the individual textile fibers).

To finalize the sensors after cutting, woven textile reinforcement handles may be placed at the sensor ends to facilitate clamping in an electromechanical tester for characterization purposes (Figure S1, Supporting Information). If desired, the sensor may also be completely encapsulated in silicone to modify its mechanical properties and provide hermetic sealing (Figure S1, Supporting Information). Compliant, robust, and low-profile connections are important for robust operation and integration into wearable sensor networks. Thin, 0.3 mm diameter, micro coaxial cables (50MCX-37, Molex Temp-Flex, USA) are used for preventing parasitic capacitance or cross-talk. Initially, a secure mechanical bond is created between the fabric and the wire with an instant adhesive (Loctite 416, Henkel, Germany), then the conductive filaments of the wire are fused to the fabric electrode surfaces with thermoplastic film (3914 Sewfree Tape, Bemis Associates Inc., USA) at 140 °C pressing for 5–10 s (Figure 1a and Movie S3, Supporting Information).

To understand sensor performance, we investigated the physical and electrical properties of the materials used in construction as well a number of sensor embodiments. Tensile force was applied in the course direction of the knit structure for characterization of the hybrid sensor and the knitted electrodes (see Figure S5, Supporting information, for the course and wale direction of a fabric). The knit fabric structure of the stretchable electrodes creates a reliable conductive network due to its interlacing conducting yarns. The resistance change range of this conductive fabric network at 0–150% strains was between 30 and 75 Ω for the given sensor dimensions, originating from relocation of the fibers and the yarns within the network. This range of resistance fluctuation contributes to a fast electrical time constant. The time constant for the sensor to charge/discharge is on the order of several nanoseconds (Figure S2, Supporting information).

Capacitance of the sensor (C_{sensor}) can be analyzed by two main components: electrode area (A) and dielectric thickness (d), in addition to the constants for dielectric permittivity of vacuum (ε_0) and permittivity of the dielectric (k). The common parallel plate capacitive sensor working mechanism relies solely on a change in dielectric thickness for silicone-based sensors.[30] However, a change in area effects capacitance change, as illustrated in Equation (1)

$$C_{\text{sensor}} = \varepsilon_0 k \frac{A}{d_0} \tag{1}$$

$$\begin{aligned} C &= \varepsilon_0 k \frac{(1+\varepsilon) l_0 (1-\nu_{\text{electrode}}\ \varepsilon) w_0}{(1-\nu_{\text{dielectric}}\ \varepsilon) d_0} \\ &\Rightarrow \nu_{\text{electrode}} = \nu_{\text{dielectric}}\ GF = (\Delta C/C_0)/\varepsilon = 1 \\ &\quad \nu_{\text{electrode}} < \nu_{\text{dielectric}}\ GF = (\Delta C/C_0)/\varepsilon > 1 \end{aligned} \tag{2}$$

When the sensor is stretched to a given strain ε, the length of capacitor increases to $(1 + \varepsilon)l_0$ while the width and thickness of the dielectric layer decrease to $(1 - (\nu_{\text{electrode}})(\Delta l/l_0))w_0$ and $(1 - (\nu_{\text{dielectric}})(\Delta l/l_0))d_0$, where l_0, w_0, and d_0 are the initial length and width of the sensor and initial thickness of dielectric layer, respectively, and $\nu_{\text{electrode}}$ and $\nu_{\text{dielectric}}$ are the Poisson's ratios for the stretchable electrodes and dielectric layer, respectively. If value of $\nu_{\text{electrode}}$ is equal to $\nu_{\text{dielectric}}$, the theoretical maximum value of the GF would be unity, which is viable for most silicone-based capacitive sensors. We investigated electrode area change corresponding to applied strain for our sensor design. For this aim, an experiment was conducted to measure the area change at specific strain intervals from drawn rectangles on the fabric, silicone, and combined sensor (**Figure 2**a,b). We observed that there is a conductive electrode area increase under applied strain due to the penetration of silicone through the mesh structure of the fabric, filling the inherent air gaps within the fabric structure which resists perpendicular shrinkage to an applied strain. Thus, under tensile load the total electrode area increases while at the same time the thickness of the dielectric layer decreases, causing an increase in capacitance. Hence, our fabric-silicone composite sensor exhibits GFs beyond unity (max. experimental finding is 1.23) due to the effect of the textile on the elastomer bulk properties (Figure 2e,f).

We also investigated the elastic behavior of the plain fabric electrode and bare silicone, as well as our sensor. We observed that the knit structure underwent 16% plastic deformation when it was stretched to 150% strain. However, introducing silicone into the fabric network contributed to an increase in the elastic region of the fabric-silicone composite structure. Plastic deformation in the composite structure was measured as 7% when it was stretched up to 150% strain as shown in Figure 2c. Also, introduction of the silicone into the fabric prevents rolling of the fabric from its edges after the stretching and relaxation cycles. Thus, more dimensionally stable structures were created (Figure S3, Supporting Information).

For characterizing the electrical response of the sensor to mechanical forces, we developed an experimental setup to collect synchronized mechanical and electrical data, using a mechanical tester (Instron 5544A, Instron, USA) and a capacitance meter (Model 3000, GLK Instruments, USA) (Figure S4, Supporting Information). Dimensions of the samples used for characterization were 80 mm × 10 mm in total area and 65 mm × 10 mm in active (stretchable) area with a dielectric thickness of 500 µm and total sensor thickness of 1.5 mm. The 500 µm dielectric thickness was chosen for optimal performance in terms of linearity and GF among several produced samples with discrete dielectric thicknesses (Table S1, Supporting Information).

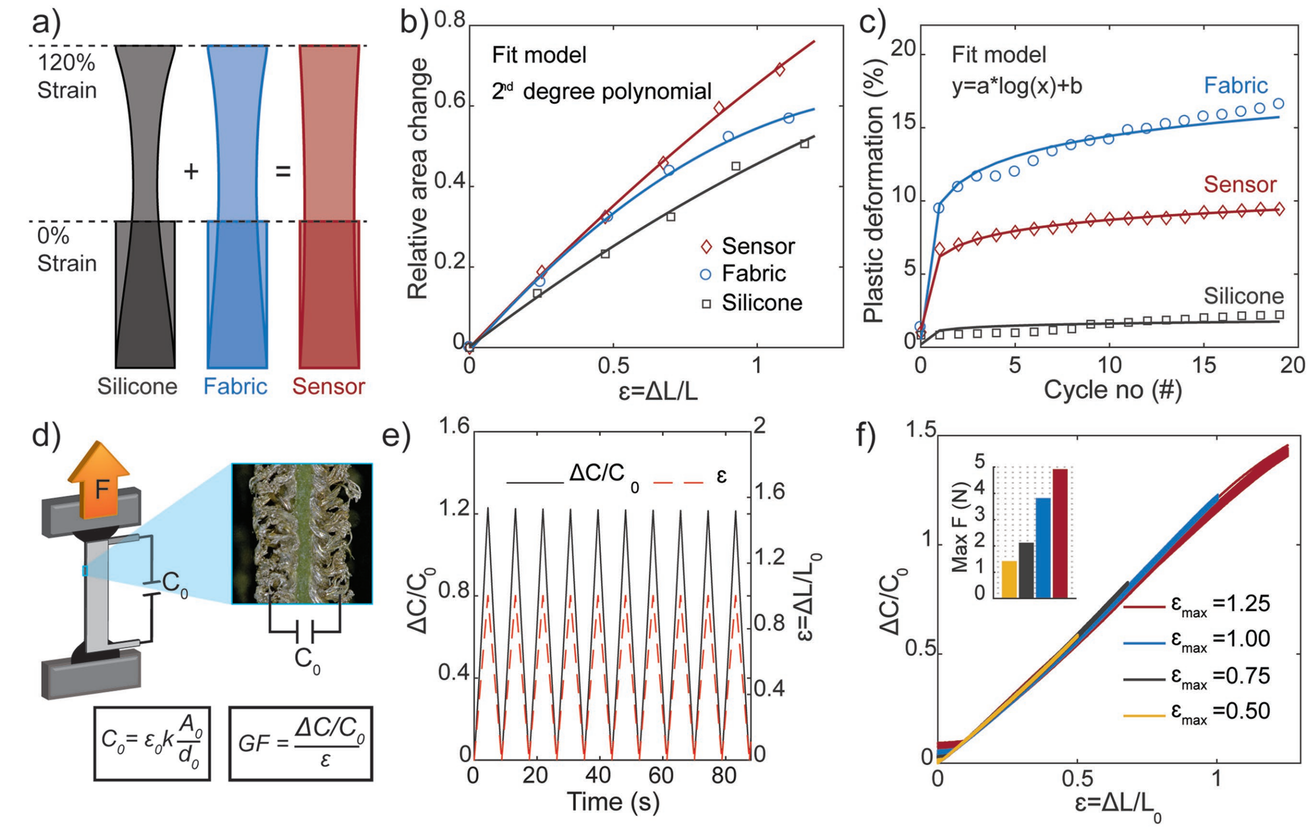

Figure 2. a) Representative sketch of area change for the sensor, the conductive fabric, and the silicone. b) Area change as a function of strain for sensor, conductive fabric, and silicone. A second-degree polynomial fit is applied to the data. c) Plastic deformation percent for the sensor, conductive fabric, and silicone. A logarithmic fit is applied to the data. d) Diagram of electromechanical test setup and cross-sectional image of the capacitive sensor. e) Relative change in sensor capacitance upon triangular cyclic straining to 100% at 0.11 Hz. f) Relative capacitance change of the sensor as a function of applied strain intervals; inset indicates max. force amount for the corresponding strain level.

We determined the strain-dependent working range of the sensor, by applying cyclic triangular strains of 50, 75, 100, and 125% at speed of 24 mm s^{-1} to the sensor. The max. hysteresis were calculated as 0, 0.2, 0.7, 1.5, and 2.5% for the applied strains at 25, 50, 75, 100, and 125%, respectively. The sensor exhibited a linear strain–capacitance relationship with limited hysteresis when cyclically stretched up to 100% applied strain. With applied strains beyond 100%, a deterioration of the signal output was observed due to increased plastic deformation of the textile, affecting linearity, GF, and hysteresis properties of the sensor (Figure 2f). Hence, we chose 100% strain level for the recommended operating range of the soft capacitive sensor and its further electromechanical characterization.

We investigated the influence of dynamic strain on the electrical performance of the sensor by stretching and releasing the sensor at 100% strain and a speed of 24 mm s^{-1}. **Figure 3**a shows the relative change in capacitance as a function of strain with a simple linear fit ($R^2 = 0.999$) and a corresponding gauge factor of 1.23. The sensor's fatigue performance was evaluated by monitoring its electrical response as a function of dynamic strain cycle number. The sample was subject to a 1000 cycle sawtooth wave profile at a speed of 24 mm s^{-1} at strain levels of $\varepsilon = 0.25$, 0.50, 0.75, and 1.00. We observed that, for strain values up to the operating range of $\varepsilon = 1.00$, a 12 and 5% decrease were observed on capacitance output at 100 and 25% strains, respectively (Figure 3b). Drifting characteristics of the sensor under static loading was also measured. Drift error was calculated as the change in the sensor capacitance response to a constant strain value. The drift values of the strain sensor found as 0.3, 0.7, 0.6, and 0.5% for the strain levels of $\varepsilon = 0.25$, 0.50, 0.75, and 1.0, respectively (Figure S6, Supporting information).

The temporal response of the textile-silicone composite sensors was determined by application of an external step-like increase in commanded strain at a speed of 24 mm s^{-1}. An increase in strain with a response time of less than 30 ms (including any delays related to instrumentation) was observed (Figure 3c). Determining the sensor bandwidth is important as the frequency of human activities can reach up to 10 Hz.[60] Hence, we performed a frequency sweep test to identify the bandwidth of the sensor. The response to increasing frequency (1–30 Hz) was monitored with a 10% strain using a DMA tester (ElectroForce 3200 Series, Bose, USA). Higher strain levels and higher frequencies could not be tested due to limitations of the machine. We found a decrease of sensor signal amplitude starting at 27 Hz (Figure 3d). Resolution of the sensor was assessed based on the noise levels at certain strain intervals up to 100% strain (more details in Table S2, Supporting Information). A resolution of 1.24% is measured at 100% strain. A moderate, monotonic decrease in absolute resolution was detected with increasing strain levels, while the relative

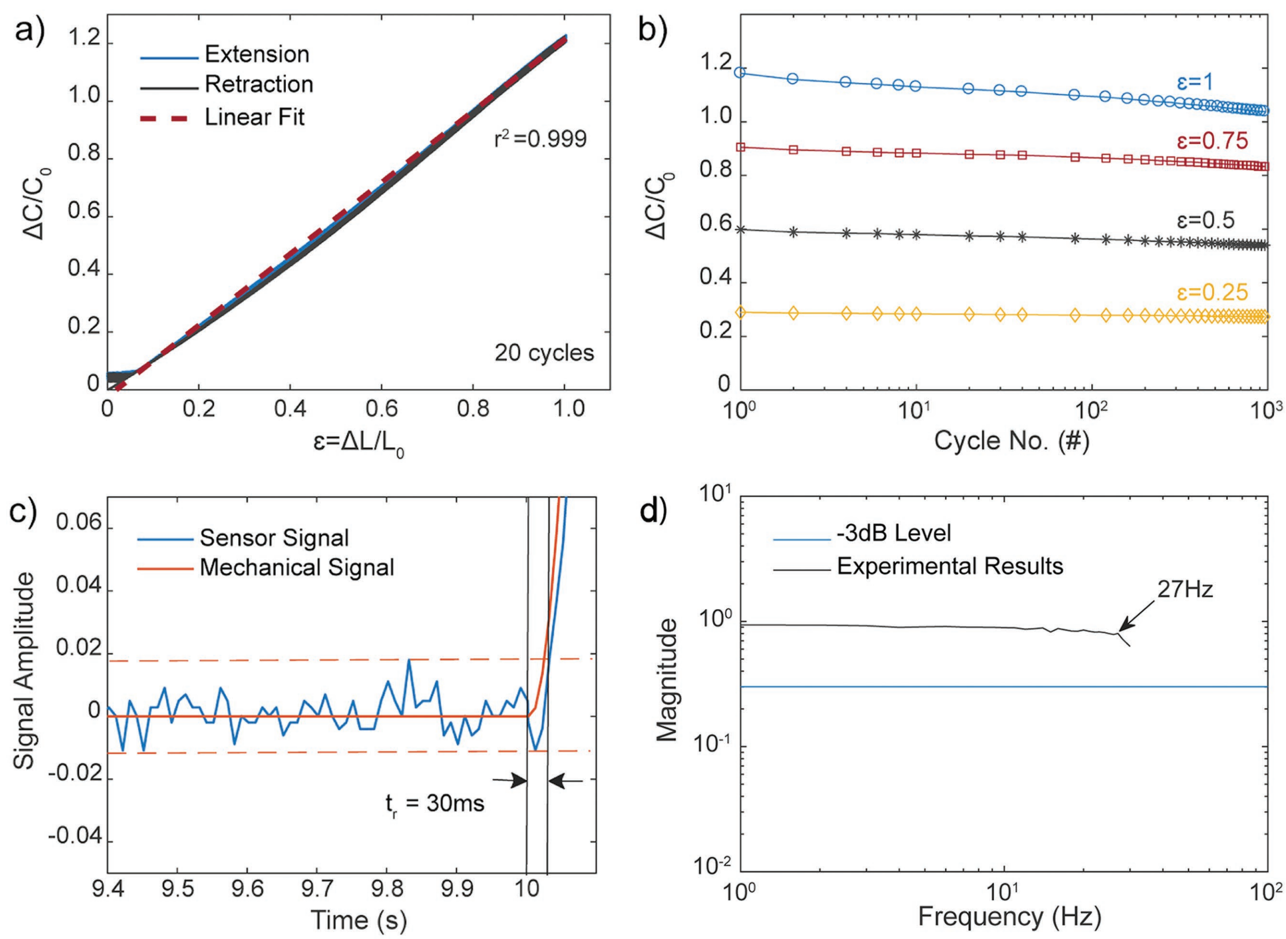

Figure 3. a) Relative capacitance change as a function of applied strain for 20 cycles. A linear fit to part of the cycles with increasing strain is presented with a red dotted line, yielding a gauge factor of 1.23. b) Relative capacitance change as a function of the cycle number for 25, 50, 75, and 100% strain levels. c) Time response of the textile-silicone composite sensors upon the application of an external step-like increase in strain load at a speed of 24 mm s^{-1}. d) Frequency sweep test: Increasing frequency from 1 to 30 Hz with the sensor stretched to 10% strain.

resolution actually improves at higher strain levels. Considering the length $L = 65$ mm of the tested sensor, absolute extensions well below half a millimeter can be detected. In addition, an electromechanical failure test was conducted by stretching the sensor up to 250% at a speed of 3 mm s^{-1}. Figure S7a,b (Supporting Information) shows that the signal is lost at 170% strain and permanent deformation occurred on sensor elasticity and the handle joints at 220% strain.

To demonstrate the potential for the composite textile-silicone sensors to be used in human motion tracking applications, they were integrated into a glove for hand motion tracking (**Figure 4**a). This use case requires moderate levels of strain (≈50%) as well as nonbulky sensors with minimal impedance due to the limited surface area available on a finger. Our scalable sensors were successfully attached to the fabric of a base glove using Ecoflex 0030. For robust electrical connections, micro coaxial cables are attached to finger-sized sensors with 40 mm × 10 mm dimensions (Figure 1). In our glove manufacturing process shown in Figure 4c, engineered areas of stiffness were extended from the sensor ends to the entire glove length. These areas maximized signal change, as only the sensors could stretch during flexion (as opposed to areas of the glove we are not measuring). We tested the sensor capacity to capture finger kinematics on a glove in real time (Figure 4d). The signal was recorded utilizing the commercially available SSM-02-13 StretchSense sensor module with Bluetooth. The capacitance change for each finger was plotted as a function of time for certain hand gestures, demonstrating the ability to track motion.

In summary, we have developed a customizable, stretchable textile-silicone composite capacitive sensor for monitoring human body articulation. Using a batch manufacturing process that combines a fabrication of a large sensor sheet and laser cutting, we demonstrate a method that can easily create sensors with consistent properties or arbitrary shapes. The network of the conductive fabric structure provides a robust and reliable electrode and the composite material produced favorable mechanical properties. Although the GF increase is minimal, this study proves that it is possible to go beyond theoretical GF limitations caused by the Poisson's ratio of the dielectric elastomer through optimizing the sensor structure. This is done by utilizing constitutive materials with Negative Poisson's ratios and can be further improved by designing an auxetic sensor structure. Our results showed that sensors exhibited high

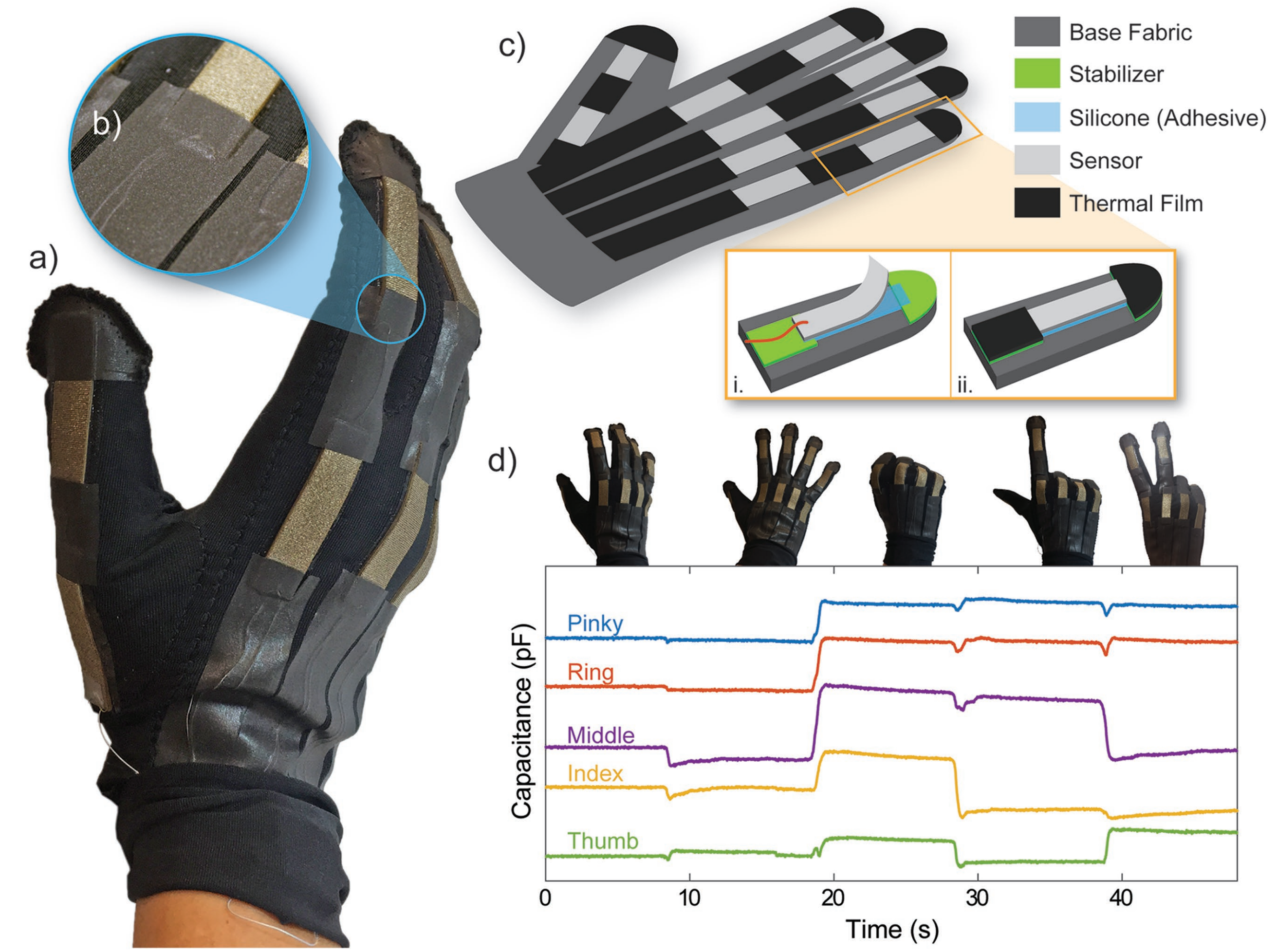

Figure 4. a) Photo of a sensing glove. b) Cable routing and strain relief are provided by the overlaid thermal film. c) Schematic diagram of the sensor placement and integration: (i) attachment of the sensor using a silicone adhesive and (ii) sensor with adhered thermal film. d) Capacitance output of the fingers during hand motion.

linearity and low hysteresis when stretched up to 100% strain with a fast response time. To make reliable measurements for an application, resolution is an important specification, related to both the sensor and the digital measurement device. Future work will involve characterizing the sensor performance if the sensor when combined with custom or off the shelf embedded electronics for wearable applications. Finally, we demonstrated that this simple and robust sensor system is very convenient for integration in/onto garments for monitoring human body activities. We envision that this type of soft strain sensor is suitable for integration into soft robots[61] and also wearable robots for assisting with mobility and grasping.[62–65]

Experimental Section

Bulk Sensor Manufacturing: Sensor mats were produced in a bulk manufacturing method for fast, scalable, and repeatable sensors (Figure 1a and Movie S1, Supporting Information). The dielectric silicone was prepared by combining SmoothOn Ecoflex 0030 parts A and B, in a 1:1 weight ratio, following the manufacturer's directions. The silicone was then mixed at 2000 rpm for 30 s and defoamed at 2200 rpm for an additional 30 s, in a centrifugal planetary mixer (ARE-310, Thinky Mixer, USA). The dielectric layer was cast from prepared silicone material using an automatic film applicator (4340, Elcometer Inc., USA) set to speed 0 with an adjustable Baker film applicator (3530/3, Elcometer Inc.) set to a height of 200 µm. The cast layer was subsequently oven cured at 70 °C for 10 min. For thinner dielectric layers, the Baker applicator was set for lower heights, and for thicker layers castings were repeated on top of the cured layer. To adhere the electrodes, additional silicone was cast upon the cured dielectric layer as an adhesive with a Baker applicator setting of 150 µm and speed setting of 0. Knit electrode material (Shieldex M-130) was hand cut to sensor mat size parallel to textile wale structure (Figure S5, Supporting Information). The knit electrode material was set on top of the uncured adhesive layer, pressed with a roller, and oven cured at 70 °C for 10 min. The sensor mat was flipped (exposing the silicone side of the dielectric layer) and the attachment process was repeated to adhere the second electrode. The sensor mat was cured, at minimum, for an additional hour at room temperature before further processing.

To shape individual sensors, masking tape (CP 101, Shurtape Technologies, LLC., USA) was affixed to the sensor mat to prevent burning. Sensors were then cut to designed size (characterization standard of 10 mm × 80 mm with incorporated connection leads) by a laser (VLS 6.60, Universal Laser Systems, USA) at 30 W power and 10% speed setting (Movie S2, Supporting Information).

Permanent Electrical Connections: Robust electrical connections were established for signal acquisition and processing for durability in wearable applications (Movie S3, Supporting Information). Micro coaxial cable (50MCX-37, Molex Temp-Flex) was stripped, and the core and sheath wire were to either electrode side of the sensor, respectively. The wires were fixed at the sensor edge with instant adhesive (Loctite 416) and cured for 15 min and then sealed with thermal seam tape (3914 Sewfree Tape) with iron at 140 °C pressed for 5–10 s.

Characterization of Mechanical Properties: Mechanical properties were tested on a commercial electromechanical tester (Instron 5544A) using a 2 kN load cell and 1 kN pneumatic grips. Load and extension data were recorded.

Plastic deformation of base materials was determined using a crosshead speed of 8 mm s^{-1} and stretching samples for 20 cycles at 120% strain. Prepared samples' dimensions were 25.4 × 76.2 mm. Thickness of fabric, silicone, and sensor samples were 450, 500 and 1400 µm, respectively.

To determine area change relative to applied strain, a rectangle was drawn on materials samples and they were stretched at specified strain intervals (0, 25, 50, 75, 100, 125, and 150%) relative to the rectangle length and held for imaging. The strained rectangle dimensions were measured using ImageJ analysis software (NIH.gov). Three sample test results were averaged.

Dynamic Electronic Characterization Testing: Sensors were dynamically tested on a commercial electromechanical tester (Instron 5544A) using a 2 kN load cell and 1 kN load-capacity pneumatic grips unless otherwise noted. Capacitance was measured with a capacitance meter (Model 3000, GLK Instruments) connected to the integrated sensor leads with probes. Via a common I/O interface, (BNC-2111, National Instruments Corp., USA), the load, extension, and capacitance data were synchronously obtained and logged. All sensors characterized were produced in a standardized size (cut to 80 mm × 10 mm with integrated connectors) and have an active, stretchable area of 65 mm × 10 mm, due to the attachment of handles. Sensors were preconditioned by stretching to 100% applied strain for minimum ten cycles. Using this setup (Figure S4, Supporting Information), characterization tests were performed on sensors.

Sensor Frequency Sweep (Bandwidth) Testing: It was performed with a using a Bose DMA, logging time, and displacement data at a 1000 Hz sampling rate. The GLK capacitance meter was connected to sensor leads with probes and was linked to an Arduino Mega 2560, acting as an analog-to-digital converter. The capacitance values were logged via Simulink software with a 100 Hz sampling rate. The mechanical tester applies a maximum of 10% strain, driven in a sinusoidal waveform (oscillating from 0% applied strain to 10%). A frequency sweep was performed from 1 to 30 Hz, with 1 Hz increments, and tens of cycling at each frequency condition. Larger maximum strains and higher frequencies could not be tested due to the displacement limitations of the machine and its setup.

Glove Manufacturing and Testing: A sensing glove was produced to understand sensor integration and motion-tracking performance. Sensors for the glove application were made following the dielectric materials and sensor production methodologies, with 150 µm thick dielectric and 40 mm × 10 mm rectangular sensor size (without integrated connectors). Electrical connections were established via the *permanent electrical connections* methodology for a durable, wearable device.

The specialized glove was designed to maximize the signal change of the sensor, and to have integrated cable routing and strain relief of wires (Figure 4a,b). Patterns including a glove base, sensor attachment points (defined from hand measurements), and areas of stiffness (required for maximized signal change and protective wiring paths) were developed using Optitex PDS 12 and Adobe Illustrator CC software. These patterns of the glove base knit textile (74861, United Knitting, USA), woven fusible stabilizer (Pellon SF101, PCP Group LLC.,USA), thermal film (Reflectivedge, Bemis Associates Inc., USA), and sensor attachment point mask (Apollo VPP100C Transparency Film, ACCO Brands, USA) were cut via laser (VLS 6.60) at settings of 10 W power and 10% speed.

Silicone was prepared using the same procedure as used in the *bulk sensor manufacturing* to use as an adhesive for the sensors. Subsequently, using the automatic film applicator at speed 0, with the Baker applicator set to 150 µm height, the silicone was applied onto the base textile that was covered with attachment point mask. Sensors with permanent connections were manually placed at each attachment point and pressed with a roller, and the entire piece was oven cured at 70 °C for 10 min. Using a combination of ironing for initial affixing, and a heat press set at 4 bar, 140 °C, for 15 s, thermal film was attached to seal stabilizer, sensor edges, and cables. Glove pattern pieces were machine-sewn together with a zigzag stitch for stretchability, using "2.5" stitch width and "3" stitch length settings. Fingertips were hand sewn using a whipstitch. Sensor cables were connected to SSM-02-13 StretchSense sensor module with Bluetooth for data acquisition during hand motions.

Supporting Information

Supporting Information is available from the Wiley Online Library or from the author.

Acknowledgements

This material is based upon the work supported by the National Science Foundation (Grant No. CBET-1454472), the Scientific and Technological Research Council of Turkey (TUBİTAK) BIDEB-2219 Postdoctoral Research program, the Defense Advanced Research Projects Agency (DARPA), Warrior Web Program (Contract No. W911NF-14-C-0051), the Wyss Institute, and the John A. Paulson School of Engineering and Applied Sciences at Harvard University. The authors would also like to thank James Weaver for SEM images.

Conflict of Interest

The authors declare no conflict of interest.

Keywords

capacitive, motion tracking, soft sensors, stretchable, textile-based sensors

Received: May 22, 2017
Published online:

[1] Y. Menguc, Y.-L. Park, E. Martinez-Villalpando, P. Aubin, M. Zisook, L. Stirling, R. J. Wood, C. J. Walsh, in *2013 IEEE Int. Conf. Robotics and Automation*, IEEE, Karlsruhe, Germany **2013**, p. 5309.
[2] Y. Mengüç, Y.-L. Park, H. Pei, D. Vogt, P. M. Aubin, E. Winchell, L. Fluke, L. Stirling, R. J. Wood, C. J. Walsh, *Int. J. Rob. Res.* **2014**, *33*, 1748.
[3] P. Gibbs, H. H. Asada, in *2004 IEEE Int. Conf. Robotics and Automation*, New Orleans, LA, USA, IEEE, **2004**, Vol. *5*, p. 4753.
[4] S. J. Preece, L. P. Kenney, M. J. Major, T. Dias, E. Lay, B. T. Fernandes, *J. NeuroEng. Rehabil.* **2011**, *8*, 32.
[5] Y. Wang, L. Wang, T. Yang, X. Li, X. Zang, M. Zhu, K. Wang, D. Wu, H. Zhu, *Adv. Funct. Mater.* **2014**, *24*, 4666.
[6] Y. Zhang, C. J. Sheehan, J. Zhai, G. Zou, H. Luo, J. Xiong, Y. T. Zhu, Q. X. Jia, *Adv. Mater.* **2010**, *22*, 3027.
[7] A. Frutiger, J. T. Muth, D. M. Vogt, Y. Mengüç, A. Campo, A. D. Valentine, C. J. Walsh, J. A. Lewis, *Adv. Mater.* **2015**, *27*, 2440.

[8] M. Amjadi, K. U. Kyung, I. Park, M. Sitti, *Adv. Funct. Mater.* **2016**, *26*, 1678.
[9] E. Roh, B.-U. Hwang, D. Kim, B. Y. Kim, N.-E. Lee, *ACS Nano* **2015**, *9*, 6252.
[10] J. H. Suh, M. Amjadi, I. Park, H. J. Yoo, *Nov. 2015 IEEE Sensors*, Busan, South Korea, IEEE, **2015**.
[11] S. Jung, J. H. Kim, J. Kim, S. Choi, J. Lee, I. Park, T. Hyeon, D. H. Kim, *Adv. Mater.* **2014**, *26*, 4825.
[12] S. M. M. De Rossi, N. Vitiello, T. Lenzi, R. Ronsse, B. Koopman, A. Persichetti, F. Giovacchini, F. Vecchi, A. J. Ijspeert, H. van Der Kooij, M. C. Carrozza, in *2010 IEEE Engineering in Medicine and Biology Conf.*, Buenos Aires, Argentina, IEEE, **2010**, p. 1279.
[13] O. Atalay, W. R. Kennon, E. Demirok, *IEEE Sens. J.* **2015**, *15*, 110.
[14] T. Q. Trung, N.-E. Lee, *Adv. Mater.* **2016**, *28*, 4338.
[15] Y.-Y. Chiu, W.-Y. Lin, H.-Y. Wang, S.-B. Huang, M.-H. Wu, *Sens. Actuators, A* **2013**, *189*, 328.
[16] Y. Chen, B. Lu, Y. Chen, X. Feng, *Sci. Rep.* **2015**, *5*, 11505.
[17] A. Atalay, O. Atalay, M. D. Husain, A. Fernando, P. Potluri, *J. Ind. Text.* **2016**, https://doi.org/10.1177/1528083716652834.
[18] L. J. Pan, A. Chortos, G. H. Yu, Y. Q. Wang, S. Isaacson, R. Allen, Y. Shi, R. Dauskardt, Z. N. Bao, *Nat. Commun.* **2014**, *5*, 8.
[19] N. Lu, C. Lu, S. Yang, J. Rogers, *Adv. Funct. Mater.* **2012**, *22*, 4044.
[20] C. Lee, L. Jug, E. Meng, *Appl. Phys. Lett.* **2013**, *102*, 5.
[21] J. T. Muth, D. M. Vogt, R. L. Truby, Y. Mengüç, D. B. Kolesky, R. J. Wood, J. A. Lewis, *Adv. Mater.* **2014**, *26*, 6307.
[22] W. Hu, X. Niu, R. Zhao, Q. Pei, *Appl. Phys. Lett.* **2013**, *102*, 38.
[23] S. D. Min, Y. Yun, H. Shin, *IEEE Sens. J.* **2014**, *14*, 3245.
[24] J. Meyer, B. Arnrich, J. Schumm, G. Troster, *IEEE Sens. J.* **2010**, *10*, 1391.
[25] D. J. Lipomi, M. Vosgueritchian, B. C. K. Tee, S. L. Hellstrom, J. A. Lee, C. H. Fox, Z. Bao, *Nat. Nanotechnol.* **2011**, *6*, 788.
[26] T. Yamada, Y. Hayamizu, Y. Yamamoto, Y. Yomogida, A. Izadi-Najafabadi, D. N. Futaba, K. Hata, *Nat. Nanotechnol.* **2011**, *6*, 296.
[27] L. Cai, L. Song, P. Luan, Q. Zhang, N. Zhang, Q. Gao, D. Zhao, X. Zhang, M. Tu, F. Yang, *Sci. Rep.* **2013**, *3*, 3048.
[28] C. Yan, J. Wang, W. Kang, M. Cui, X. Wang, C. Y. Foo, K. J. Chee, P. S. Lee, *Adv. Mater.* **2014**, *26*, 2022.
[29] G.-W. Huang, H.-M. Xiao, S.-Y. Fu, *Sci. Rep.* **2015**, *5*, 8801.
[30] X. Li, R. Zhang, W. Yu, K. Wang, J. Wei, D. Wu, A. Cao, Z. Li, Y. Cheng, Q. Zheng, R. S. Ruoff, H. Zhu, *Sci. Rep.* **2012**, *2*, 870.
[31] X. Xiao, L. Yuan, J. Zhong, T. Ding, Y. Liu, Z. Cai, Y. Rong, H. Han, J. Zhou, Z. L. Wang, *Adv. Mater.* **2011**, *23*, 5440.
[32] F. Xu, Y. Zhu, *Adv. Mater.* **2012**, *24*, 5117.
[33] M. Amjadi, A. Pichitpajongkit, S. Lee, S. Ryu, I. Park, *ACS Nano* **2014**, *8*, 5154.
[34] S. Tadakaluru, W. Thongsuwan, P. Singjai, *Sensors* **2014**, *14*, 868.
[35] S. Yao, Y. Zhu, *Nanoscale* **2014**, *6*, 2345.
[36] C.-X. Liu, J.-W. Choi, *Microelectron. Eng.* **2014**, *117*, 1.
[37] B.-U. Hwang, J. H. Lee, T. Q. Trung, E. Roh, D.-I. Kim, S. W. Kim, N.-E. Lee, *ACS Nano* **2015**, *9*, 8801.
[38] D. Kang, P. V. Pikhitsa, Y. W. Choi, C. Lee, S. S. Shin, L. Piao, B. Park, K.-Y. Suh, T.-I. Kim, M. Choi, *Nature* **2014**, *516*, 222.
[39] B.-C. Zhang, H. Wang, Y. Zhao, F. Li, X.-M. Ou, B.-Q. Sun, X. H. Zhang, *Nanoscale* **2016**, *8*, 2123.
[40] J. Park, Y. Lee, J. Hong, Y. Lee, M. Ha, Y. Jung, H. Lim, S. Y. Kim, H. Ko, *ACS Nano* **2014**, *8*, 12020.
[41] Z. Liu, D. Qi, P. Guo, Y. Liu, B. Zhu, H. Yang, Y. Liu, B. Li, C. Zhang, J. Yu, B. Liedberg, X. Chen, *Adv. Mater.* **2015**, *27*, 6230.
[42] Y. Wang, R. Yang, Z. Shi, L. Zhang, D. Shi, E. Wang, G. Zhang, *ACS Nano* **2011**, *5*, 3645.
[43] M. Hempel, D. Nezich, J. Kong, M. Hofmann, *Nano Lett.* **2012**, *12*, 5714.
[44] J. J. Park, W. J. Hyun, S. C. Mun, Y. T. Park, O. O. Park, *ACS Appl. Mater. Interfaces* **2015**, *7*, 6317.
[45] D. H. Ho, Q. Sun, S. Y. Kim, J. T. Han, D. H. Kim, J. H. Cho, *Adv. Mater.* **2016**, *28*, 2601.
[46] J. Zhao, G. Wang, R. Yang, X. Lu, M. Cheng, C. He, G. Xie, J. Meng, D. Shi, G. Zhang, *ACS Nano* **2015**, *9*, 1622.
[47] V. Tsouti, V. Mitrakos, P. Broutas, S. Chatzandroulis, *IEEE Sens. J* **2016**, *16*, 3059.
[48] X. Guo, Y. Huang, X. Cai, C. Liu, P. Liu, *Meas. Sci. Technol.* **2016**, *27*, 4.
[49] A. Nelson, G. Singh, R. Robucci, C. Patel, N. Banerjee, *IEEE Trans. Multi-Scale Comput. Syst.* **2015**, *1*, 62.
[50] T. Hoffmann, B. Eilebrecht, S. Leonhardt, *IEEE Sens. J* **2011**, *11*, 1112.
[51] Y. Cheng, R. Wang, J. Sun, L. Gao, *Adv. Mater.* **2015**, *27*, 7365.
[52] C. R. Merritt, H. T. Nagle, E. Grant, *IEEE Sens. J.* **2009**, *9*, 71.
[53] C. M. Yang, T. L. Yang, C. C. Wu, S. H. Hung, M. H. Liao, M. J. Su, H. C. Hsieh, in *2014 IEEE Int. Conf. Consumer Electronics*, Las Vegas, NV, USA, IEEE, **2014**, Vol. *232*, p. 33.
[54] J. Lee, H. Kwon, J. Seo, S. Shin, J. H. Koo, C. Pang, S. Son, J. H. Kim, Y. H. Jang, D. E. Kim, *Adv. Mater.* **2015**, *27*, 2433.
[55] S. C. Mannsfeld, B. C. Tee, R. M. Stoltenberg, C. V. H. Chen, S. Barman, B. V. Muir, A. N. Sokolov, C. Reese, Z. Bao, *Nat. Mater.* **2010**, *9*, 859.
[56] S. Han, S. Hong, J. Ham, J. Yeo, J. Lee, B. Kang, P. Lee, J. Kwon, S. S. Lee, M. Y. Yang, *Adv. Mater.* **2014**, *26*, 5808.
[57] P. K. Yang, L. Lin, F. Yi, X. Li, K. Pradel, Y. Zi, C. Wu, J. He, Y. Zhang, Z. Wang, *Adv. Mater.* **2015**, *27*, 3817.
[58] S. J. Park, J. Kim, M. Chu, M. Khine, *Adv. Mater. Technol.* **2016**, *1*, 1600053.
[59] K.-I. Jang, S. Y. Han, S. Xu, K. E. Mathewson, Y. Zhang, J.-W. Jeong, G.-T. Kim, R. C. Webb, J. W. Lee, T. J. Dawidczyk, R. H. Kim, Y. M. Song, W.-H. Yeo, S. Kim, H. Cheng, S. I. Rhee, J. Chung, B. Kim, H. U. Chung, D. Lee, Y. Yang, M. Cho, J. G. Gaspar, R. Carbonari, M. Fabiani, G. Gratton, Y. Huang, J. A. Rogers, *Nat. Commun.* **2014**, *5*, 4779.
[60] H. Zeng, Y. Zhao, *Sensors* **2011**, *11*, 638.
[61] D. Holland, E. Park, P. Polygerinos, G. Bennett, C. Walsh, *Soft Rob.* **2014**, *1*, 224.
[62] F. A. Panizzolo, I. Galiana, A. T. Asbeck, C. Siviy, K. Schmidt, K. G. Holt, C. J. Walsh, *J. NeuroEng. Rehabil.* **2016**, *13*, 43.
[63] P. Polygerinos, Z. Wang, K. C. Galloway, R. J. Wood, C. J. Walsh, *Rob. Auton. Syst.* **2015**, *73*, 135.
[64] H. Zhao, K. O'Brien, S. Li, R. F. Shepherd, *Science Robotics* **2016**, *1*, eaai7529.
[65] J. Bae, S. M. M. De Rossi, K. O'Donnell, K. L. Hendron, L. N. Awad, T. R. T. Dos Santos, V. L. De Araujo, Y. Ding, K. G. Holt, T. D. Ellis, presented at *Aug. 2015 IEEE Int. Conf. Rehabilitation Robotics (ICORR)*, Singapore, Singapore, **2015**.